Essential role of Glu-C66 for menaquinol oxidation indicates transmembrane electrochemical potential generation by *Wolinella succinogenes* fumarate reductase

C. Roy D. Lancaster[†‡], Roland Groß[§], Alexander Haas[†], Michaela Ritter[¶], Werner Mäntele[¶], Jörg Simon[§], and Achim Kröger[§]

[†]Max Planck Institute of Biophysics, Department of Molecular Membrane Biology, Heinrich-Hoffmann-Strasse 7, D-60528 Frankfurt am Main, Germany; [§]Institut für Mikrobiologie, Johann Wolfgang Goethe-Universität, Marie-Curie Strasse 9, D-60439 Frankfurt am Main, Germany; and [¶]Institut für Biophysik, Johann Wolfgang Goethe-Universität, Theodor-Stern-Kai 7, Haus 74, D-60590 Frankfurt am Main, Germany

Communicated by Hartmut Michel, Max Planck Institute of Biophysics, Frankfurt, Germany, September 6, 2000 (received for review August 8, 2000)

Quinol:fumarate reductase (QFR) is a membrane protein complex that couples the reduction of fumarate to succinate to the oxidation of quinol to quinone, in a reaction opposite to that catalyzed by the related enzyme succinate:quinone reductase (succinate dehydrogenase). In the previously determined structure of QFR from *Wolinella succinogenes*, the site of fumarate reduction in the flavoprotein subunit A of the enzyme was identified, but the site of menaquinol oxidation was not. In the crystal structure, the acidic residue Glu-66 of the membrane spanning, diheme-containing subunit C lines a cavity that could be occupied by the substrate menaquinol. Here we describe that, after replacement of Glu-C66 with Gln by site-directed mutagenesis, the resulting mutant is unable to grow on fumarate and the purified enzyme lacks quinol oxidation activity. X-ray crystal structure analysis of the Glu-C66 → Gln variant enzyme at 3.1-Å resolution rules out any major structural changes compared with the wild-type enzyme. The oxidation-reduction potentials of the heme groups are not significantly affected. We conclude that Glu-C66 is an essential constituent of the menaquinol oxidation site. Because Glu-C66 is oriented toward a cavity leading to the periplasm, the release of two protons on menaquinol oxidation is expected to occur to the periplasm, whereas the uptake of two protons on fumarate reduction occurs from the cytoplasm. Thus our results indicate that the reaction catalyzed by *W. succinogenes* QFR generates a transmembrane electrochemical potential.

Succinate:quinone reductases (SQRs) and quinol:fumarate reductases (QFRs) catalyze the oxidation of succinate to fumarate with concomitant reduction of quinone to hydroquinone (quinol) as well as the reverse reaction. SQR (respiratory complex II) is involved in aerobic metabolism as part of the citric acid cycle and the aerobic respiratory chain (1). QFR is involved in anaerobic respiration with fumarate as the terminal electron acceptor (2, 3) and is part of the electron transport chain catalyzing the oxidation of various donor substrates (e.g., NADH, H_2, or formate) by fumarate. These reactions are coupled via an electrochemical proton gradient to ADP phosphorylation with inorganic phosphate by ATP synthase.

QFR and SQR complexes are collectively referred to as succinate:quinone oxidoreductases (EC 1.3.5.1) and are predicted to share similar structures. The complexes consist of two hydrophilic and one or two hydrophobic, membrane-integrated subunits (reviewed in ref. 4). The larger hydrophilic subunit A carries covalently bound FAD and subunit B contains three iron-sulfur centers. QFR of *Wolinella succinogenes* and SQR of *Bacillus subtilis* contain only one hydrophobic subunit (C) with two heme *b* groups. In contrast, SQR and QFR of *Escherichia coli* contain two hydrophobic subunits (C and D), which bind either one (SQR) or no heme *b* group (QFR). The structure of *W. succinogenes* QFR has been determined at 2.2-Å resolution [Protein Data Bank (PDB) entry 1QLA; ref. 5]. One of the heme groups, the "proximal" heme b_P is located close to the negative side of the membrane and the iron-sulfur subunit B. The other, the "distal" heme b_D is oriented away from subunit B and close to the positive side of the membrane. The two heme groups have different oxidation-reduction potentials (6), one is the "high-potential" heme b_H, the other the "low-potential" heme b_L. Although Hägerhäll and coworkers (7) have assigned b_P and b_D in *B. subtilis* SQR to correspond to b_H and b_L, respectively, it has not yet been established which of the hemes b_D and b_P corresponds to b_L and which one to b_H in *W. succinogenes* QFR.

In the *W. succinogenes* QFR crystal structure, the site of fumarate reduction in the flavoprotein subunit A of the enzyme was identified (PDB entry 1QLB; ref. 5), but the site of menaquinol oxidation was not. The coordinate file 1FUM for the heme-free *E. coli* QFR, determined at a resolution of 3.3 Å (PDB entry 1FUM; ref. 8), contains two menaquinone models per QFR, but structural alignment (5) shows that these are at positions occupied by the heme propionates in *W. succinogenes* QFR.

In the absence of a reliably defined crystal structure for the binding of menaquinol to *W. succinogenes* QFR, we attempted to identify the site of menaquinol oxidation by a different approach. The rationale for initiating the present experiments is illustrated in Fig. 1. In the original structure of *W. succinogenes* QFR, two cavities (depicted in purple) were detected that are located in the region of subunit C, which is oriented toward the periplasm. The upper cavity is too hydrophobic to bind the menaquinol head-group because no obvious hydrogen bonding partners are apparent. The lower cavity is too polar, particularly in its lower part, to contain the quinol head group, but could contain water molecules not resolved in the electron density. However, the accessible areas of the two cavities are separated by only 5 Å. The introduction of the menaquinol head group in this region could be accommodated by changes in the side-chain positions of a

---

Abbreviations: b_D, distal heme; b_H, high-potential heme; b_L, low-potential heme; b_P, proximal heme; NCS, noncrystallographic symmetry; QFR, quinol:fumarate reductase; $DMNH_2$, 2,3-dimethyl-1,4-naphthoquinol; SQR, succinate:quinone reductase; PDB, Protein Data Bank.

Data deposition: The atomic coordinates of the Glu-C66 → Gln *Wolinella succinogenes* mutant QFR have been deposited in the Protein Data Bank, http://www.rcsb.org (PDB ID code 1E7P).

[‡]To whom reprint requests should be addressed. E-mail: Roy.Lancaster@mpibp-frankfurt.mpg.de.

Article published online before print: *Proc. Natl. Acad. Sci. USA*, 10.1073/pnas.220425797. Article and publication date are at www.pnas.org/cgi/doi/10.1073/pnas.220425797

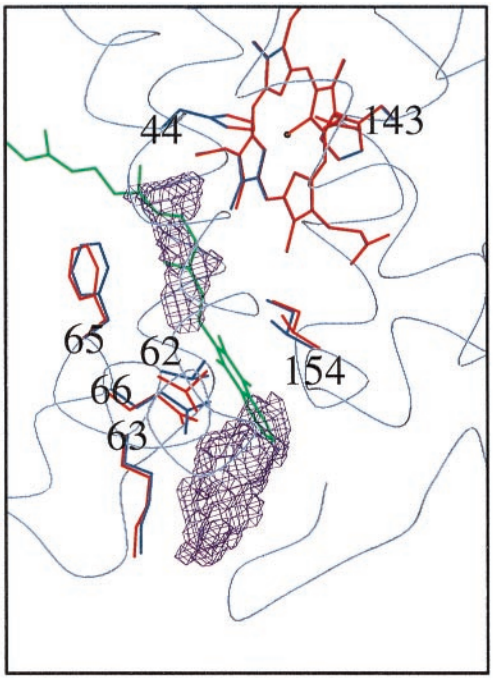

Fig. 1. A working hypothesis. Two distal cavities (purple) in subunit C of the original structure of *W. succinogenes* QFR (PDB entry 1QLA) as detected with the program VOIDOO (33) and a working model of menaquinol binding (green) are shown. To accommodate the quinol head group in its current tentative position between the cavities, amino acid side-chain movements from their original positions (blue) to positions drawn in red are required as derived from energy minimization simulations with CNS. The heme group shown is the distal heme b_D. In this orientation, the periplasm is at the bottom and the rest of the QFR complex extends beyond the top and the right of the figure. Figs. 1, 2, and 4 were prepared with a version of MOLSCRIPT (34) modified for color ramping (35) and map drawing (36) capabilities.

small number of amino acid residues by movements in the order of 1 Å. Side-chain movements on this scale have been experimentally observed for the removal of ubiquinone from the secondary acceptor quinone (Q_B) site of the photosynthetic reaction center from *Rhodopseudomonas viridis* (9). In the orientation shown in Fig. 1, the menaquinol could donate a hydrogen bond from one of its hydroxyl groups to a carboxylate oxygen of the side chain of the residue Glu-C66.

This model prompted us to investigate the possible role of Glu-C66 for *W. succinogenes* QFR. Here we describe the effects of replacing Glu-C66 with Gln by site-directed mutagenesis. We conclude that Glu-C66 is an essential constituent of the menaquinol oxidation site. The consequences of this finding are discussed.

Materials and Methods

Mutagenesis. The mutant *W. succinogenes* FrdC-E66Q was constructed by transforming *W. succinogenes* Δ*frdCAB* with a derivative of pFrdcat2 (10). Plasmid pFrdcat2 contains the entire *frdCAB* operon and integrates into the genome of *W. succinogenes* Δ*frdCAB* by homologous recombination (10). Plasmid pFrdcat2-E66Q was synthesized by using the QuikChange site-directed mutagenesis kit (Stratagene) with pFrdcat2 as template and a specifically synthesized complementary primer pair [forward primer: 5′-(3000)CCAAGAAATTTCAGCTAGACTTC ATCTTTGAGGG-3′; numbering according to the sequence deposited in the GenBank database under accession no. AJ000662]. The altered nucleotide is printed in bold and the resulting glutamine codon is underlined. Cells of *W. succinogenes* Δ*frdCAB* grown with formate and nitrate were used for transformation as described (10). Transformants were selected on agar plates with a medium containing kanamycin (25 mg/liter) and chloramphenicol (12.5 mg/liter). The integration of plasmid pFrdcat2-E66Q into the genome of *W. succinogenes* Δ*frdCAB* was confirmed by Southern blot analysis as described (10). The mutation was confirmed and unwanted mutations were ruled out by sequencing a PCR product containing the *frdC* gene that was obtained by using genomic DNA of the mutant strain as template and a specifically synthesized primer pair.

Cell Growth and Purification of QFR. *W. succinogenes* was grown with formate as electron donor and either fumarate or nitrate as electron acceptor as described (11, 12). The latter medium was supplemented with Brain-Heart-Infusion [0.5% (mass/vol), GIBCO/BRL]. Fumarate reductase activities were measured with cell homogenates from bacteria grown with formate and nitrate (10). The enzymic activities listed in Table 1 were measured at 37°C according to Unden and Kröger (13). Protein was determined by using the Biuret method with KCN (14). QFR was isolated as described (15) with modifications reported previously (5). The amount of heme *b* reduced by 2,3-dimethyl-1,4-naphthoquinol ($DMNH_2$) or by dithionite was calculated from the absorbance difference between the reduced and the oxidized sample at 565 nm minus that at 575 nm using the molar extinction coefficient of 23.4 $mM^{-1} \cdot cm^{-1}$ (6).

Crystallization of QFR. Before crystallization, Glu-C66 → Gln QFR was further purified by preparative flat-bed isoelectric focusing as described for the wild-type enzyme (5). Monoclinic crystals, space group $P2_1$, were grown by sitting drop vapor diffusion as described (5), except that the detergent concentra-

Table 1. Growth and enzymatic activities of *W. succinogenes* wild-type and FrdC-E66Q cells and properties of the isolated fumarate reductases

	Strain wild type	Strain FrdC-E66Q
Doubling time (h) with		
Formate + fumarate	1.6	∞
Formate + nitrate	1.5	1.5
Fumarate reductase activity (units mg^{-1} cell protein)		
Succinate → methylene blue	0.31	0.17
Fumarate reductase activity of isolated enzyme (units mg^{-1} protein)		
Succinate → methylene blue	28.8	16.9
$DMNH_2$ → fumarate	7.4	≤0.01
Heme *b* of isolated enzyme reduced by (μmol g^{-1} protein)		
$DMNH_2$	3.8	0.5
Dithionite	7.2	7.0

Table 2. Data collection and refinement statistics of the Glu-C66 → Gln QFR form C crystal

	Overall	Highest resolution shell
Resolution range, Å	30.0–3.10	3.29–3.10
R_{sym},[*] %	6.0	26.0
$I/\sigma\ I$	11.9	2.0
No. of reflections used (completeness)	102,882 (80.8%)	12,962 (61.7%)
In working set	102,132 (80.1%)	12,867 (61.0%)
In test set	750 (0.7%)	95 (0.7%)
R_{free},[†] %	29.3	47.3
R_{cryst},[‡] %	28.5	48.0
Luzzati coor. error,[§] Å	0.66	

No. of nonhydrogen atoms with occupancy > 0 in the model	9,271
Protein atoms	9,077
Heterogen atoms	194
Solvent atoms	0
B factor from Wilson plot, Å²	65.4
Average *B* factor, Å²	86.2
$n_{\text{obs}}/n_{\text{par}}$[¶]	1.57
rms deviations from ideal values[‖]	
Bonds, Å	0.012
Bond angles, °	1.6
Torsional angles, °	22.5
Improper torsional angles, °	1.73

[*] $R_{\text{sym}} = \Sigma_{\text{i,hkl}} \mid <I(\text{hkl})> - I_{\text{i}}(\text{hkl}) \mid \Sigma_{\text{i,hkl}} I_{\text{i}}(\text{hkl})$.

[†] $R_{\text{free}} = \Sigma_{\text{hkl})\ \varepsilon\text{T}} \mid |F_{\text{o}}| - |F_{\text{c}}| \mid / \Sigma_{\text{hkl})\ \varepsilon T} |F_{\text{o}}|$, where *T* is the test set (38).

[‡] $R_{\text{cryst}} = \Sigma_{(\text{hkl})} \mid |F_{\text{o}}| - |F_{\text{c}}| \mid / \Sigma_{(\text{hkl})} |F_{\text{o}}|$.

[§] Estimate of the mean coordinate error from a Luzzati plot (39).

[¶] n_{obs} = number of observed unique reflections used in the working set; n_{par} = number of parameters necessary to define the model; this includes three parameters (*x*, *y*, *z* coordinates) per atom plus four (isotropic atomic *B* factors for the four NCS related atoms).

[‖] Based on protein parameter files (40), heme cofactor parameter files (9), and parameter files generated for the other prosthetic groups (5).

tions were lowered to 0.01% dodecyl-β-D-maltoside and 0.10% decylmaltoside with 1.2% benzamidine.

Data Collection and Analysis. X-ray data collection was carried out at European Synchrotron Radiation Facility beamline BM14 (λ = 0.958 Å, T = 2–4°C), Grenoble. Intensity data were obtained by using a charge-coupled device detector (MAR Research, Hamburg). Only one crystal was required for the data set listed in Table 2. Data were processed with the HKL programs DENZO and SCALEPACK (16) with a cutoff of $-1.0\ \sigma$ on intensities. The structural model for crystal form A was used as a search model for phase determination of crystal form C by molecular replacement with the program CNS (17). Rigid body refinement, simulated annealing, followed by conventional positional refinement and restrained individual *B* factor refinement, were performed by using the program CNS. The atomic model of QFR was rebuilt by using O (18). Strict noncrystallographic symmetry (NCS) constraints were applied between the four QFR monomers in the asymmetric unit for positional refinement, but no NCS restraints were applied for *B* factor refinement.

Spectroelectrochemical Redox Titration. The QFR sample in 100 mM phosphate buffer, pH 7, containing 100 mM KCl and 3.2 mM dodecyl-β-D-maltoside was concentrated to approximately 0.8 mM by using a 100-kDa Microcon filtration cell (Amicon). The redox titrations were performed in an ultra-thin-layer spectroelectrochemical cell (optical path length was of the order of 10 μm) that was designed for UV/visible and IR spectrometry (19, 20). The surface of the gold grid working electrode was modified with a mercaptopropionic acid solution (2 mM in ethanol) to prevent protein adsorption. To enable fast equilibration of the redox reaction, a mixture of 15 redox mediators (tetrachlorobenzoquinone; 2,6-dichlorophenol-indophenol; ruthenium hexaminchloride; 1,2-naphthoquinone; trimethylhydroquinone; menadione; 2-hydroxy-1,4-naphthoquinone; anthraquinone-2-sulfonate; benzyl viologen; methyl viologen; neutral red; 5-hydroxy-1,4-naphthoquinone; duroquinone; anthraquinone; and anthraquinone-2,6-disulphonate) was added to the protein solution, thus covering a (midpoint) potential range from −0.42 V to 0.28 V. The total concentration of each mediator substance in the experiment was approximately 40 μM. This was high enough to guarantee fast equilibration, but sufficiently low to avoid significant spectral contributions to the cytochrome *b* measurement. The spectroelectrochemical cell was filled with 8–9 μl of protein solution. The applied potentials were measured with an Ag/AgCl/3 M KCl reference electrode but all quoted values are potentials versus standard hydrogen electrode at pH 7.

Absorbance difference spectra in the range of 400 to 700 nm were recorded at 5°C by using a dispersive spectrometer that has been described in previous reports (20, 21). Difference spectra were obtained by applying an initial potential at which the two hemes (b_{H}, b_L) were either fully reduced or fully oxidized. Then a single-beam spectrum was measured and taken as a reference for subsequent potential steps that covered the potential range between fully reduced and fully oxidized. Before recording the respective single-beam spectrum after changing the potential by 25 mV, the protein was given 5–6 min to equilibrate, although, because of the various mediators, the very thin layer of protein solution and the gold grid surface modification, equilibration times were of the order of 1 min. The titration curves were generated on the basis of the redox dependence of the amplitudes of the Soret and α-band, respectively. To obtain values for the midpoint potentials of heme b_{H} and heme b_{L}, iterative fitting of a calculated Nernst function (22) was performed.

Results and Discussion

Construction and Properties of the Strain *W. succinogenes* FrdC-E66Q and the Isolated Enzyme Glu-C66 → Gln QFR. The mutant strain FrdC-E66Q is compared with the wild type in Table 1. The mutant did not grow with fumarate as the terminal electron acceptor; however, it did grow as fast as the wild type when nitrate replaced fumarate. As assayed with succinate oxidation by methylene blue, activities of the mutant cell homogenate and the isolated enzyme were comparable to those of the wild type. The activity monitored by this assay is independent of the diheme subunit C (15). However, when fumarate reductase activity was assayed by monitoring fumarate reduction by DMNH_2, which is diheme-subunit C-dependent (15), it was not detectable in the case of Glu-C66 → Gln QFR. In the wild-type enzyme, half of the dithionite-reducible heme *b* could be reduced by DMNH_2, which has a midpoint potential of −75 mV (6). In Glu-C66 → Gln QFR, heme *b* reduction by DMNH_2 was negligible (see Table 1).

To investigate the nature of these dramatic effects, the Glu-C66 → Gln QFR was crystallized, and x-ray diffraction data were collected as described in *Materials and Methods*. Under the reported crystallization conditions, three different crystal forms have been observed for the wild-type enzyme, all of them monoclinic, space group $P2_1$. Two of them, crystal form A (a = 85.2 Å, b = 189.0 Å, c = 117.9 Å, β = 104.5°), and crystal form B (a = 118.4 Å, b = 85.1 Å, c = 188.9 Å, β = 96.5°) have resulted in successful structure determinations (5). The data for the third crystal form, form C (compare below), have so far been of insufficient quality and completeness for structural analysis of the wild-type enzyme (C.R.D.L., unpublished observations).

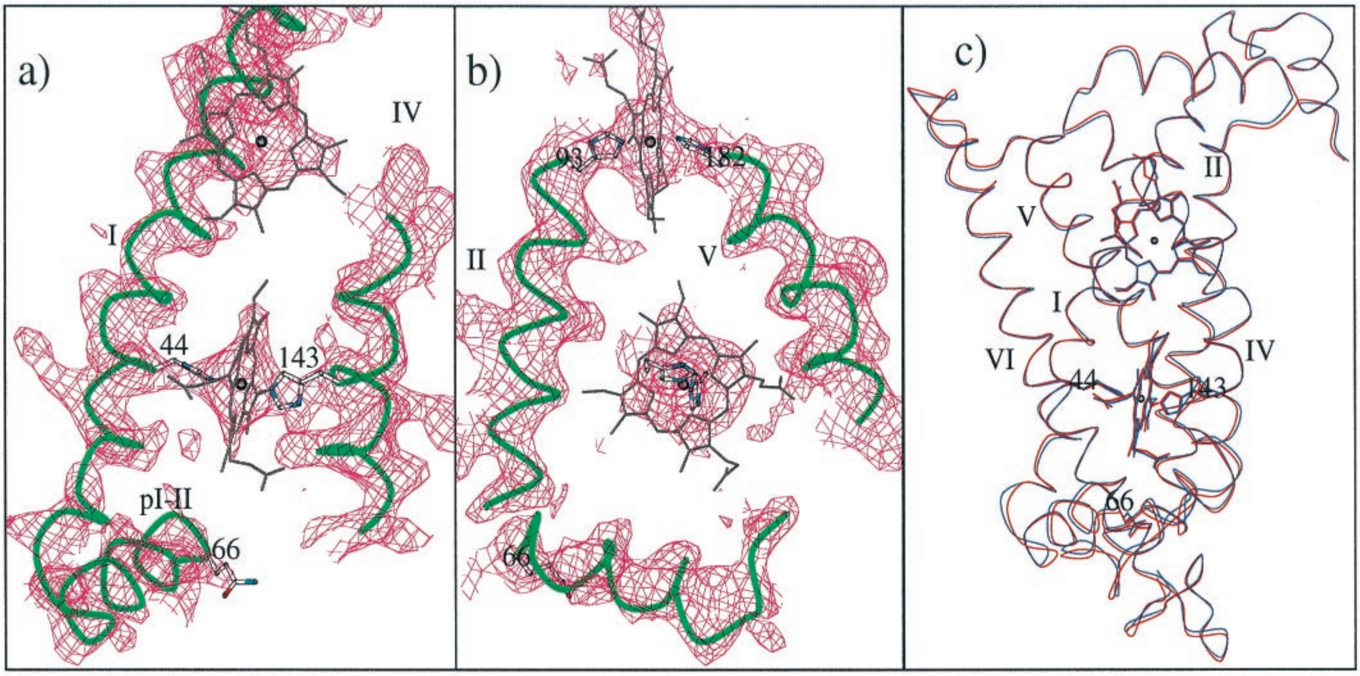

Fig. 2. The crystal structure of Glu-C66 → Gln QFR. (*a* and *b*) Representative sections of the $2|F_o|-|F_c|$ composite-omit electron density map, contoured at 1.0 standard deviations (σ) above the mean density of the map. Shown are the two heme groups, b_P (*Upper*) and b_D (*Lower*), in subunit C, as well as the periplasmic helix pI-II with its C-terminal extension containing the exchanged residue C66 (*a* and *b*). Drawn in green are the Cα traces of the transmembrane helices I and IV (*a*) and II and V (*b*) that form the four-helix bundle enclosing the two heme groups (5). To reduce overlap, the upper ends of helices IV, II, and V have been omitted. (*c*) Comparison of the heme positions and the Cα traces for the C subunits of wild-type QFR (blue, PDB entry 1QLA) and Glu-C66 → Gln QFR (red). The rms deviation for the 254 Cα atoms in the C subunit models is 0.44 Å.

However, the only useful Glu-C66 → Gln QFR data set was collected on crystals of form C with unit cell dimensions $a = 81.1$ Å, $b = 290.2$ Å, $c = 153.6$ Å, and $\beta = 95.7°$. In contrast to the two other crystal forms, which have two QFR complexes in the asymmetric unit, the asymmetric unit of this crystal form contains four QFR complexes.

Using the structural model for crystal form A (PDB entry 1QLA) as a search model for phase determination by molecular replacement, one QFR dimer ($R_{\text{cryst}} = 45.8\%$) could be identified by clear, unique solutions of the rotation and translation searches, and the position of a second QFR dimer was readily determined from its iron positions as the highest peaks in an $|F_o|-|F_c|$ difference electron density map ($R_{\text{cryst}} = 37.6\%$). Using the data between 30.0- and 3.1-Å resolution, refinement of the model containing 9,077 protein atoms and another 194 heterogen atoms for the prosthetic groups was performed. Strict NCS constraints on the atomic positions were imposed, but no NCS restraints were applied for *B*-factor refinement, resulting in a ratio of the number of independent observations to the number of parameters in the model, $n_{\text{obs}}/n_{\text{par}}$ of 1.57. The crystallographic *R* factor and the free *R* factor dropped to 28.5% and 29.3%, respectively. Control calculations showed that R_{cryst} could be further lowered significantly by removal of the NCS constraints. However, this did not reflect an improvement of the accuracy of the structure, as R_{free} did not improve. The drop in R_{cryst} was attributed to overfitting of the structure, with $n_{\text{obs}}/n_{\text{par}}$ dropping to 0.39. Thus the model is discussed on the basis of the statistics displayed in Table 2.

The relatively high *R* factors in the higher-resolution shells (compare Table 2) were attributed to the high degree of anisotropy in the diffraction pattern with the crystal diffracting to better than 2.8 Å along the b* and c* axes, but considerably weaker (≈3.8 Å) along the a* axis. Nevertheless, the electron density map, calculated with the composite-omit protocol for the removal of model bias (23), as shown in Fig. 2 *a* and *b*, clearly allows us to confirm the general structure of Glu-C66 → Gln QFR. With the coordinate error estimated to be 0.66 Å (see Table 2), no significant differences compared with the wild-type enzyme structure are observed (rms deviation = 0.49 Å for 1,041 Cα atoms) with the exception of regions of subunit A, which appear to have a slightly different orientation relative to the rest of the complex (not shown). This can be attributed to the different packing in crystal form C and will be presented in detail elsewhere. In summary, the crystal structure determination rules out that any major structural changes could explain the loss of menaquinol oxidation activity in Glu-C66 → Gln QFR.

Redox Titration. To investigate whether the effect of the Glu-C66 → Gln exchange could be indirect by changing the oxidation-reduction potential of the heme groups, the latter was determined by analyzing electrochemically induced absorbance difference spectra at the wavelengths of 428 nm (Soret band) and 561 nm (α-band). For both wild-type QFR and Glu-C66 → Gln QFR, both the reductive titration of the oxidized enzyme and the oxidative titration of the reduced enzyme are shown in Fig. 3 together with the fitted calculated Nernst function. Two titrating groups, i.e., heme b_H and heme b_L, can be clearly identified in each of the curves. Within an error of 5%, the two hemes contributed equally to the total change in absorbance. Taking the average value of reductive and oxidative titrations, the fitted Nernst functions yielded midpoint potentials of $E_{\text{m,bL}} = -152$ mV and $E_{\text{m,bH}} = -9$ mV for wild-type QFR and $E_{\text{m,bL}} = -142$ mV and $E_{\text{m,bH}} = -14$ mV for Glu-C66 → Gln QFR. The error in the determination of the midpoint potentials can be estimated to be ± 10 mV from the standard deviation of several performed redox titrations. Analogous titration curves based on the amplitudes of the α-band yielded the same values for the midpoint potentials quoted above. Thus we conclude that the introduced

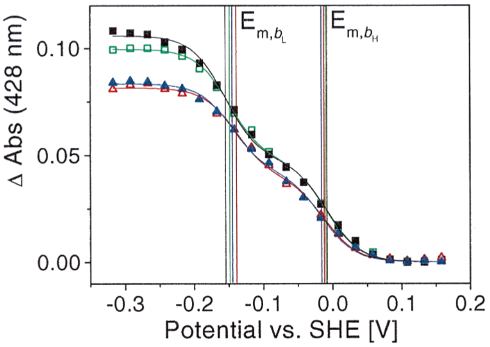

Fig. 3. The oxidation-reduction potentials of heme b_H and b_L in wild-type QFR and Glu-C66 → Gln QFR. Electrochemical redox titrations of wild-type QFR (squares) and Glu-C66 → Gln QFR (triangles). The amplitude of the Soret band maximum at 428 nm is plotted as a function of the applied potential: open symbols correspond to an oxidative titration, full symbols correspond to a reductive titration. To avoid overlap, absorbance differences are displayed as measured and have not been scaled according to the cytochrome *b* concentration. The black and green curves show a reversible titration of wild-type QFR, blue and red refer to Glu-C66 → Gln QFR. Fitting to calculated Nernst curves yielded the following individual values for the midpoint potentials E_m of hemes b_L and b_H, with the first value determined from the reductive titration and the second from the oxidative titration. For wild-type QFR: $E_{m,bL} = -155$ mV and -149 mV; $E_{m,bH} = -8$ mV and -10 mV. For Glu-C66 → Gln QFR: $E_{m,bL} = -145$ mV and -139 mV; $E_{m,bH} = -16$ mV and -12 mV, as indicated by the vertical colored lines. SHE, standard hydrogen electrode.

mutation did not significantly alter the midpoint potential of either heme b_L or heme b_H.

Conclusions

Our conclusions are summarized in Fig. 4. The lack of any significant structural change observed in the 3.1-Å resolution Glu-C66 → Gln QFR crystal structure and the lack of any significant effect of the Glu-C66 → Gln exchange on the oxidation-reduction potentials of the heme groups indicate that the dramatic effects on the enzymic activity of the altered QFR cannot be explained other than by concluding that Glu-C66 is an essential constituent of the menaquinol oxidation site. Most probably, this residue acts by accepting a quinol proton during electron transfer from the quinol to the distal heme b_D. Glu-C66 lines a cavity that extends to the periplasmic aqueous phase. This strongly suggests that the protons liberated during menaquinol oxidation are released on the periplasmic side of the membrane. Because the protons consumed in the concomitant reduction of fumarate are taken up from the cytoplasmic side, quinol oxidation by fumarate should be coupled to the generation of an electrochemical proton potential across the membrane. However, in previous experiments, quinol oxidation by fumarate was found to be apparently electroneutral in intact bacteria, with inverted vesicles or liposomes containing *W. succinogenes* QFR (24). These results were interpreted to indicate that the protons released in quinol oxidation were liberated to the cytoplasm. The interpretation is in striking contrast to the location of the site of quinol oxidation close to Glu-C66. Considering the evidence presented here, it is very difficult to envisage proton conduction from the quinol site close to Glu-C66 to the cytoplasmic side of the membrane.

Succinate oxidation by menaquinone, an endergonic reaction under standard conditions, is catalyzed by a SQR in *B. subtilis.* This enzyme is similar to *W. succinogenes* QFR also with respect to the diheme cytochrome *b* (or C) subunit. From the location of the four histidine residues ligating the heme groups, the structure of this C subunit was concluded to be similar to that of *W. succinogenes* (25). The residue corresponding to Glu-C66 in *W. succinogenes* QFR, which also is conserved in the QFR enzymes from the ε-proteobacteria *Campylobacter jejuni* (26) and *Helicobacter pylori* (27, 28), is an Asp in *B. subtilis* SQR (25) and may be located close to the site of menaquinone reduction, which has been proposed to be located close to the heme b_D (29). There is experimental evidence indicating that succinate oxidation by menaquinone is electrogenic in *B. subtilis* and is driven by the electrochemical proton potential (30). This is the analogous reaction to that presented here for *W. succinogenes* QFR (Fig. 4), but in the opposite direction (31, 32).

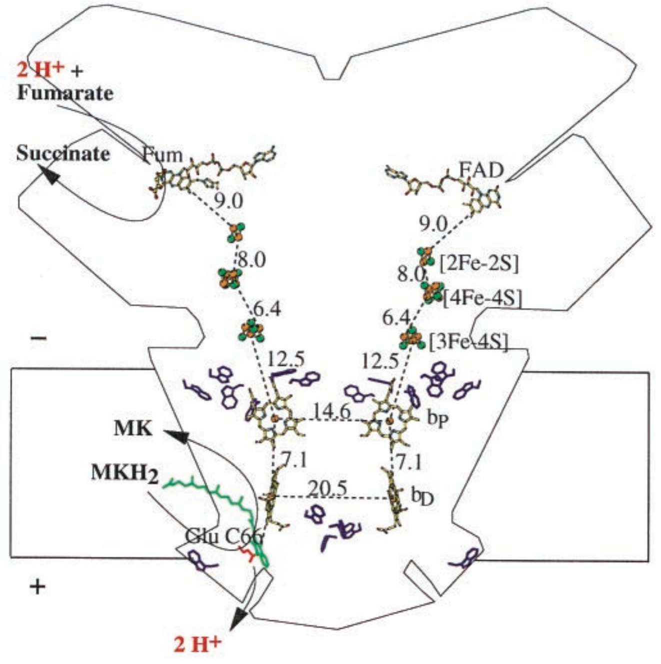

Fig. 4. Transmembrane electrochemical potential generation by *W. succinogenes* QFR coupling the two-electron oxidation of menaquinol (MKH_2) to menaquinone (MK) to the two-electron reduction of fumarate to succinate. The positive (+) and negative (−) sides of the membrane are indicated. The prosthetic groups of the QFR dimer are displayed (coordinate set PDB entry 1QLA; ref. 5). Distances between prosthetic groups are edge-to-edge distances in Å as defined in ref. 37. Distances shorter than 14 Å (i.e., within one QFR monomer, but not between the two monomers of the dimer) are considered to be relevant for physiological electron transfer. Also drawn are the side chains of Glu-C66 (in red) and of the subunit C Trp residues (purple). The latter are markers for the hydrophobic surface-to-polar transition zone of the membrane. The position of bound fumarate (Fum) is taken from PDB entry 1QLB (5). The tentative model of menaquinol binding (drawn in green) is taken from Fig. 1. Its edge-to-edge distance to heme b_D is 6.7 Å.

We thank Oliver Schürmann and Monica Sänger (both at Institut für Mikrobiologie), Annette Roth (Max Planck Institute of Biophysics), and Christine Ernd (Institut für Biophysik) for technical assistance and Ed Mitchell (European Synchrotron Radiation Facility) for support during data acquisition at European Synchrotron Radiation Facility Grenoble beamline BM14. This work was supported by the Deutsche Forschungsgemeinschaft (SFB 472, Grants P19, P5, and P21) and the Max-Planck-Gesellschaft.

1. Saraste, M. (1999) *Science* **283,** 1488–1493.
2. Kröger, A. (1978) *Biochim. Biophys. Acta* **505,** 129–145.
3. Kröger, A., Geisler, V., Lemma, E., Theis, F. & Lenger, R. (1992) *Arch. Microbiol.* **158,** 311–314.
4. Hägerhäll, C. (1997) *Biochim. Biophys. Acta* **1320,** 107–141.
5. Lancaster, C. R. D., Kröger, A., Auer, M. & Michel, H. (1999) *Nature (London)* **402,** 377–385.
6. Kröger, A. & Innerhofer, A. (1976) *Eur. J. Biochem.* **69,** 497–506.
7. Hägerhäll, C., Fridén, H., Aasa, R. & Hederstedt, L. (1995) *Biochemistry* **34,** 11080–11089.

8. Iverson, T. M., Luna-Chavez, C., Cecchini, G. & Rees, D. C. (1999) *Science* **284,** 1961–1966.
9. Lancaster, C. R. D. & Michel, H. (1997) *Structure (London)* **5,** 1339–1359.
10. Simon, J., Gross, R., Ringel, M., Schmidt, E. & Kröger, A. (1998) *Eur. J. Biochem.* **251,** 418–426.
11. Bronder, M., Mell, H., Stupperich, E. & Kröger, A. (1982) *Arch. Microbiol.* **131,** 213–223.
12. Lorenzen, J. P., Kröger, A. & Unden, G. (1993) *Arch. Microbiol.* **159,** 477–483.
13. Unden, G. & Kröger, A. (1981) *Eur. J. Biochem.* **120,** 577–584.
14. Bode, C., Goebell, H. & Stähler, E. (1968) *Z. Klin. Chem. Klin. Biochem.* **6,** 419–422.
15. Unden, G., Hackenberg, H. & Kröger, A. (1980) *Biochim. Biophys. Acta* **591,** 275–288.
16. Otwinowski, Z. & Minor, W. (1997) *Methods Enzymol.* **276,** 307–326.
17. Brünger, A. T., Adams, P. D., Clore, G. M., DeLano, W. L., Gros, P., Grosse-Kunstleve, R. W., Jiang, J.-S., Kuszewski, J., Nilges, M., Pannu, N. S., *et al*. (1998) *Acta Crystallogr. D* **54,** 905–921.
18. Jones, T. A., Zou, J. Y., Cowan, S. W. & Kjeldgaard, M. (1991) *Acta Crystallogr. A* **47,** 110–119.
19. Moss, D. A., Nabedryk, E., Breton, J. & Mäntele, W. (1990) *Eur. J. Biochem.* **187,** 565–572.
20. Mäntele, W. (1996) in *Biophysical Techniques in Photosynthesis*, eds. Hoff, A. J. & Amesz, J. (Kluwer, Dordrecht, The Netherlands), pp. 137–160.
21. Mäntele, W. (1993) *Trends Biochem. Sci.* **18,** 197–202.
22. Baymann, F., Moss, D. A. & Mäntele, W. (1991) *Anal. Biochem.* **199,** 269–274.
23. Hodel, A., Kim, S.-H. & Brünger, A. T. (1992) *Acta Crystallogr. A* **48,** 851–859.
24. Geisler, V., Ullmann, R. & Kröger, A. (1994) *Biochim. Biophys. Acta* **1184,** 219–226.
25. Hägerhäll, C. & Hederstedt, L. (1996) *FEBS Lett.* **389,** 25–31.
26. Parkhill, J., Wren, B. W., Mungall, K., Ketley, J. M., Churcher, C., Basham, D., Chillingworth, T., Davies, R. M., Feltwell, T., Holroyd, S., *et al*. (2000) *Nature (London)* **403,** 665–668.
27. Tomb, J.-F., White, O., Kerlavage, A. R., Clayton, R. A., Sutton G. G., Fleischmann, R. D., Ketchum, K. A., Klenk, H.-P., Gill, S., Dougherty, B. A., *et al*. (1997) *Nature (London)* **388,** 539–547.
28. Ge, Z., Jiang, Q., Kalisiak, M. S. & Taylor, D. E. (1997) *Gene* **204,** 227–234.
29. Matsson, M., Tolstoy, D., Aasa, R. & Hederstedt, L. (2000) *Biochemistry* **39,** 8617–8624.
30. Schirawski, J. & Unden, G. (1998) *Eur. J. Biochem.* **257,** 210–215.
31. Ohnishi, T., Moser, C. C., Page, C. C., Dutton, P. L. & Yano, T. (2000) *Structure (London)* **8,** R23–R32.
32. Lancaster, C. R. D. & Kröger, A. (2000) *Biochim. Biophys. Acta* **1459,** 422–431.
33. Kleywegt, G. J. & Jones, T. A. (1994) *Acta Crystallogr. D* **50,** 175–185.
34. Kraulis, P. J. (1991) *J. Appl. Crystallogr.* **24,** 946–950.
35. Esnouf, R. M. (1997) *J. Mol. Graphics Mod.* **15,** 132–134.
36. Esnouf, R. M. (1999) *Acta Crystallogr. D* **55,** 938–940.
37. Page, C. C., Moser, C. C., Chen, X. & Dutton, P. L. (1999) *Nature (London)* **402,** 47–52.
38. Brünger, A. T. (1992) *Nature (London)* **355,** 472–475.
39. Luzzati, P. V. (1952) *Acta Crystallogr.* **5,** 802–810.
40. Engh, R. A. & Huber, R. (1991) *Acta Crystallogr. A* **47,** 392–400.